Accounting for crack closure effects in TMF crack growth tests with extended hold times in gas turbine blade alloys

Jordi Loureiro, Per Almroth, Frans Palmert, David Gustafsson, Kjell Simonsson, Robert Eriksson and Daniel Leidermark

Loureiro, J., Almroth, P., Palmert, F., Gustafsson, D., Simonsson, K., Eriksson, R., Leidermark, D., (2021), Accounting for crack closure effects in TMF crack growth tests with extended hold times in gas turbine blade alloys, *International Journal of Fatigue*, 142, .
https://doi.org/10.1016/j.ijfatigue.2020.105917

International Journal of Fatigue

Accounting for crack closure effects in TMF crack growth tests with extended hold times in gas turbine blade alloys

Jordi Loureiro-Homs[1*], Per Almroth[2], Frans Palmert[2], David Gustafsson[2], Kjell Simonsson[1], Robert Eriksson[1], Daniel Leidermark[1]

[1] *Division of Solid Mechanics, Linköping University, Sweden*

[2] *Siemens Energy, Finspång, Sweden*

[*] *Corresponding author. Email: jordi.loureiro@liu.se*

Abstract: Crack closure effects are known to have a large impact on crack growth behaviour. In this work, tests were performed on Inconel 792 specimens under TMF loading conditions at 100-850 °C with extended hold times at tensile stress. The effective stress-intensity range was estimated experimentally using a compliance-based method leading to the conclusion that crack closure appears to have a primary impact on the crack growth behaviour for this material under the conditions studied. The crack closure behaviour for the tests was successfully modelled using numerical simulations, including creep.

Keywords: crack propagation, Inconel 792, thermomechanical fatigue, turbine blade, crack closure, compliance, node release.

1 Introduction

Since the early seventies, when Elber showed the influence of crack closure in fatigue crack growth [1,2], a great amount of work has been done proving the importance of this phenomenon. New experimental techniques, such as digital image correlation (DIC), have also enabled to understand the actual mechanical conditions around the crack tip, reaffirming the importance of this phenomenon [3].

The experimental work reported in [4] shows that crack closure effects can explain, to a large degree, the differences in crack growth rates for different hold times and load ratios on a single-crystal nickel-based superalloy for blade applications. These results fostered the hypothesis that crack closure effects might also have a large effect in other nickel-based turbine blade materials, such as the alloy Inconel 792, and thus are central for explaining the effect of different load ratios and also different hold times under TMF loading conditions. A similar work in [5] also highlighted the importance of crack closure on this material under out-of-phase (OP) thermomechanical loading, concluding that crack closure effects can explain the observed higher crack growth rates compared to room temperature tests at the same external loads.

The present work is intended to investigate three main topics; first, the crack opening stress is estimated experimentally using a compliance-based approach. Secondly, the numerical models are verified against the experimental estimations of crack closure, and third, with the aid of the numerical model, the crack opening levels are refined by obtaining the displacement at a location near the crack-tip and the results are used to discuss, with a better resolution, the influence of crack closure in this material and test conditions.

Previous work related to residual stress was carried out for Inconel 792 in [6,7]. The results showed that under TMF conditions, initial plastic strains have a large impact on crack growth rates, especially for cases undergoing large initial deformations. The residual stress arising from the plastic deformation on the uncracked body, are limited though, to cases where most of the inelastic strains occur at the first few cycles if they are to be used to explain the crack growth rate. In some sense, the current work is an

extension to the mentioned work. A distinction between residual stress and plasticity-induced crack closure is often found in the published literature [8], albeit the underlying mechanism is shared for both [9]. Residual stress (and its related initial plastic deformations) are commonly understood as the consequence of initial plastic deformations on the uncracked body, whereas plasticity-induced crack closure is understood as the plastic deformations occurring at the crack flanks as it propagates through the material. In both cases, ultimately is the inelastic deformations occurring around the crack that induce a certain level of stress which in turn facilitate or hinder the opening of the crack tip.

In this work, several TMF experimental tests for Inconel 792 were carried out and post-processed, following the methodology detailed in [4] to calculate the effective stress intensity factor, ΔK_{eff}. The preliminary evaluation of the experimental results using ΔK_{eff} show that crack closure is a relevant phenomenon although alone, it cannot completely explain the behaviour under all different load ratios and hold times as it can do for the material described in [4]. This is particularly true for longer hold times, where an explanation for the differences in crack growth rate can be oxidation or creep effects.

2 Material and crack growth testing

The material tested is the polycrystalline conventionally-cast nickel-base superalloy IN792. This material was subjected to hot isostatic pressing at 1195°C and 150 MPa for 3 h. A two-step ageing process is performed first by a solution heat treatment at 1121 ºC for 2 h and second by ageing at 845ºC for 24 h. All specimens are machined from cast round bars to the two geometries shown in Figure 1. This polycrystalline nickel-based super-alloy is mostly used for precision cast turbine blades and vanes, due to the combination of excellent mechanical properties at elevated temperatures along with corrosion and oxidation resistance. It is categorized as coarse-grained. The grain sizes typically range from 1 to 3 mm, even though it can be noted that for thin-walled castings, finer grain size is obtained. A cross-section of an Inconel 792 round bar, etched and polished, observed under the stereo-microscope is shown in Figure 2. In the specimens machined from round bars, the grain size is 1-3 mm.

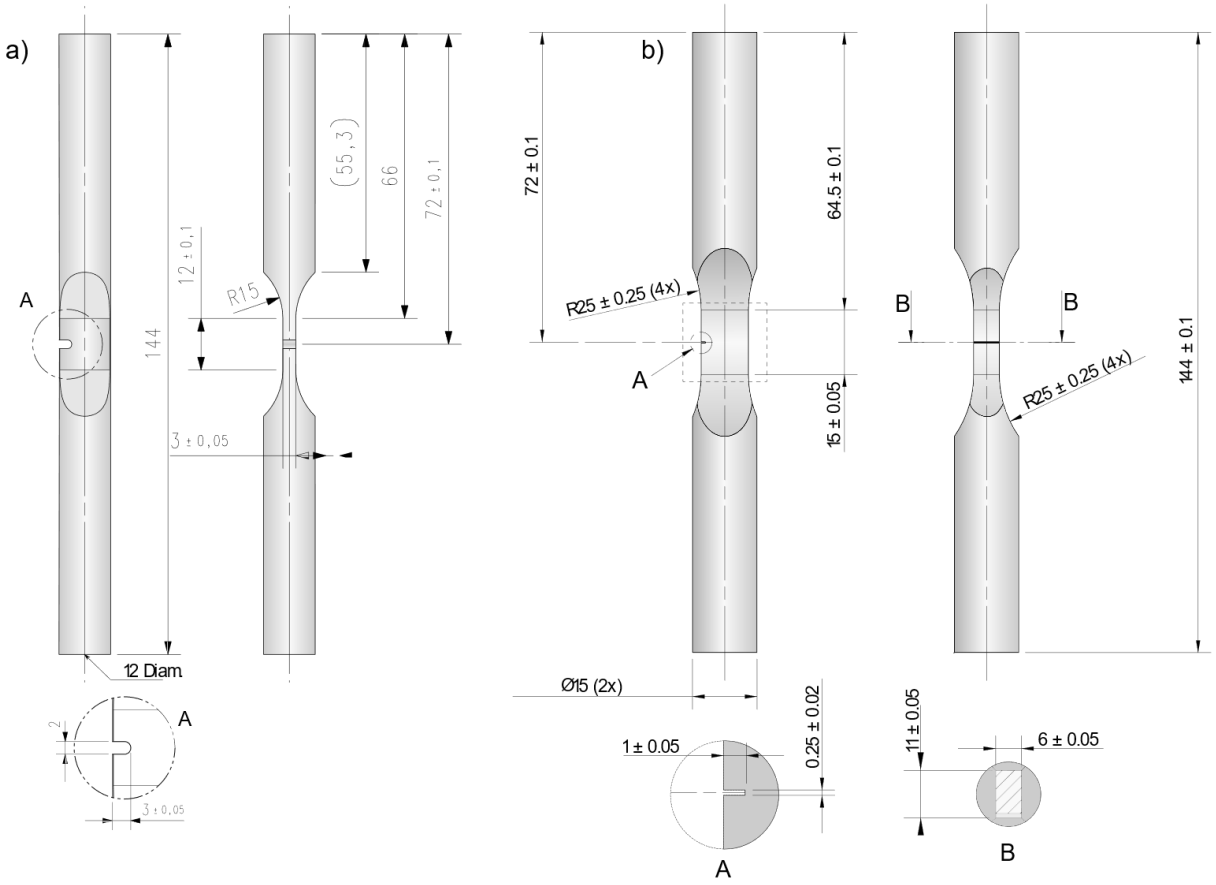

Figure 1: Test specimens geometries used for experimental crack growth tests: a) SEN-1 and b) SEN-2.

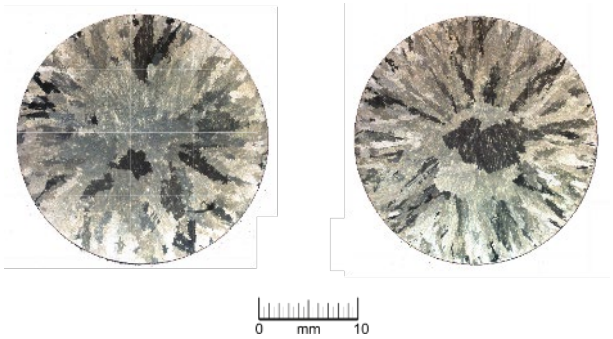

Figure 2: Transversal cross-section of two round bar samples, showing the typical grain size.

The testing was performed using a test setup identical to the one described in [4], using a 100kN servo-hydraulic machine. The heating of the specimen was done by induction-heating and cooling was performed using compressed air from two nozzles. The heating and cooling were set to a constant rate of 2 °C/s. This temperature rate was controlled with a spot-welded thermocouple, located in the centre of the specimen, on the opposite side of the notch. Before the testing campaign, the uniformity of the temperature on the rectangular cross-section was verified using a specimen subjected to the thermal cycle with at least 6 thermocouples distributed within the gauge section. The temperature variation was within +/-20°C if the entire gauge section is considered, and significantly smaller if the region where the crack propagates was considered. The displacements were measured with an extensometer located on the same side as the notch, with a length of 12mm.

Testing conditions

Pre-cracking was achieved by isothermal cycling at elevated temperature until a Mode I crack of at least 0.8mm, measured from the notch root, was created. This pre-cracking cycle was also utilised to obtain isothermal crack growth data. In some cases, several testing blocks at different load levels were used for the same specimen, usually during the isothermal pre-cracking stages. The test matrix for this work is shown in Table 1. All the tests are stress-controlled, including the hold time. The stress ratio R is defined as the minimum applied nominal stress over the maximum nominal stress.

Table 1: List of performed experiments.

Test ID	Geometry	Test type	T range [°C]	σ ratio, R	Hold time
LCF00177	SEN-1	Isothermal	850	-1	0
TMF00151	SEN-1	IP-TMF	100-850	-1	1 h
TMF3912	SEN-1	IP-TMF	100-850	-1	1 h
TMF00182	SEN-1	IP-TMF	100-850	-1	1 h
TMF4208	SEN-2	IP-TMF	100-850	-1	6 h

Crack length measurement by the compliance method

The crack length evaluation was done through post-processing the test data; in-situ crack length measurements were done to monitor the crack growth. This post-process is thoroughly described in [10]. In short, the crack length is correlated to the decrease in the relative stiffness of the specimen during each cycle. This method has been proven to provide good results, after comparison with heat tints and optical measurements at the sides of the specimens, although it relies on the assumption that, during the unloading cycle, the material behaviour is linear-elastic. Also worth noting is that the relative stiffness drop accounts for an average crack length, and that the presence of secondary cracks might also influence the accuracy of the method for high-temperature, long dwell tests in which secondary cracks are more likely.

3 Experimental crack opening evaluation

The experimental evaluation method of crack closure under TMF loading conditions, using a compliance-based method is described in [11], and has since been further developed, [4]. The method described in [4] has been used in this work, and in short, it takes into account the variation in elastic modulus as a function of temperature, which is a major difference compared to the previously published work reported in [11]. Furthermore, this closure evaluation method does not rely on the assumption of linear-elastic behaviour throughout the entire loading cycle; this assumption is only made for the part of the loading ramp where the crack is closed, as well as the start of the unloading when the crack is open. The stiffness of the specimen is calculated using the displacement measured by the extensometer pins located 6 mm away from the notch root, therefore the method does not account for the local opening of the crack tip but rather the apparent global crack opening. Thus, the estimated stress intensity range ΔK_{eff} obtained experimentally needs to be understood as an approximation. A further discussion about this topic is included in the upcoming results section.

The degree of crack opening, D_i, is obtained by the ratio of the relative stiffness drop of the specimen during the loading cycle i $(\beta_{i,load})$, with the relative stiffness drop for the fully open crack during the unloading cycle $i-1$, $\left(\beta_{i-1,unload}\right)$ as described by,

$$D_i(\tau) = \frac{\beta_{i,load(\tau)}}{\beta_{i-1,unload}} = \frac{1-\frac{M_{i,load(\tau)}}{M_{0,load}\left(T_i(\tau)\right)}}{1-\frac{M_{i-1,unload}}{M_{0,unload}}} \quad (1)$$

Fel! Bokmärket är inte definierat.

Where τ is a dimensionless time variable,

$$\tau = \frac{t-t_i}{t_{ramp}} \quad (2)$$

The denominator in Equation 1 can be interpreted as the relative stiffness drop in cycle i, evaluated for a specific point on the unloading ramp. The numerator is the relative stiffness drop in cycle i, evaluated continuously throughout the loading ramp, from minimum to maximum load. The experimental evaluation does not require any material input other than the characterisation of the specimen's uncracked stiffness $\left(M_{0,unload}\right)$ and the uncracked stiffness as a function of the temperature $M_{(0,load)}\left(T_i(\tau)\right)$. Note that the specimen's uncracked stiffness, $M_{0,unload}$ and the unloading stiffness, $M_{i-1,unload}$ are evaluated at the same point through the cycle and therefore the variation in elastic modulus has no influence on the evaluation as these two points are at the same temperature. An illustration of the typical evaluation of M_{load} and M_{unload} is included in Figure 3.

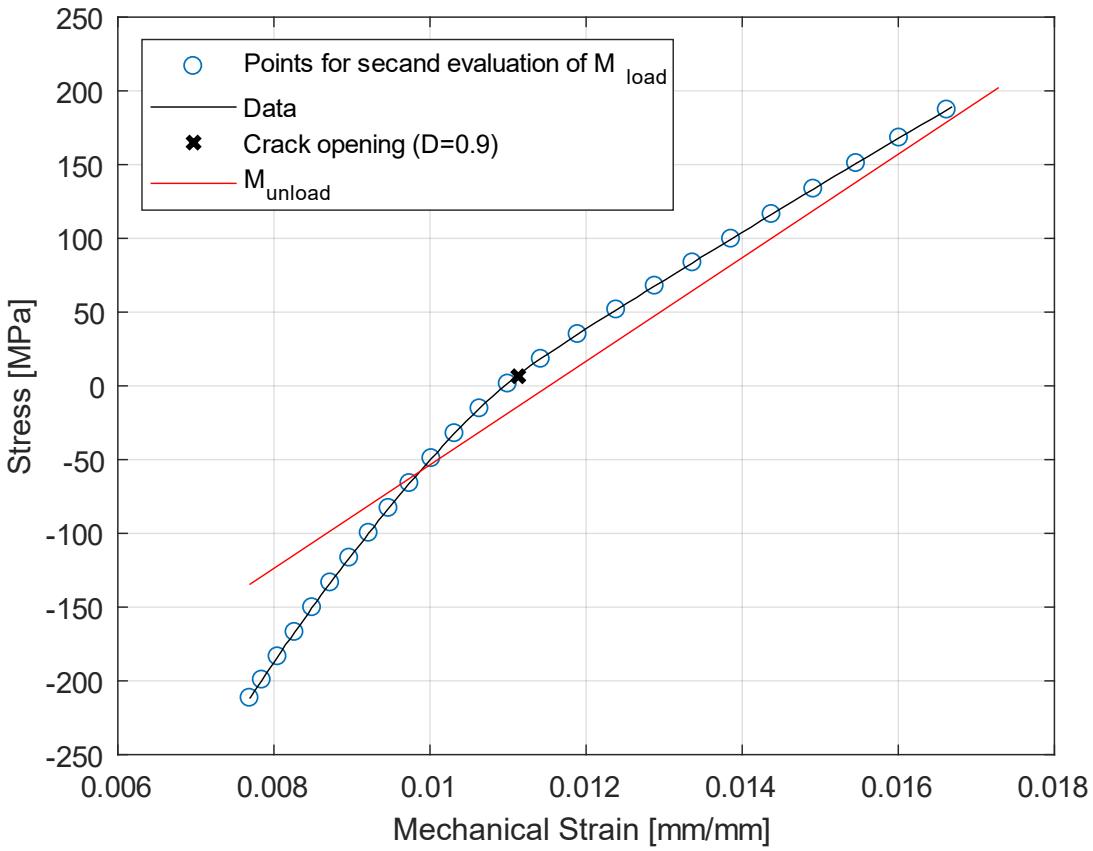

Figure 3: Illustration of the typical evaluation of M_{load} for a cracked specimen. The secant evaluation is performed on the points obtained by filtering by means of a central moving average of the raw data.

The value of D ranges from 0 to 1, corresponding to a fully closed and a fully opened crack, respectively. D is evaluated for the entire loading ramp although it is during the lower part of the loading and up until the crack is fully open that it is considered valid based on the assumption that the specimen has an elastic response up until that point. After that, the inelastic response may change the meaning of the degree of opening and it may no longer be a useful measure for that purpose. The evolution of the crack opening parameter D is illustrated in Figure 4.

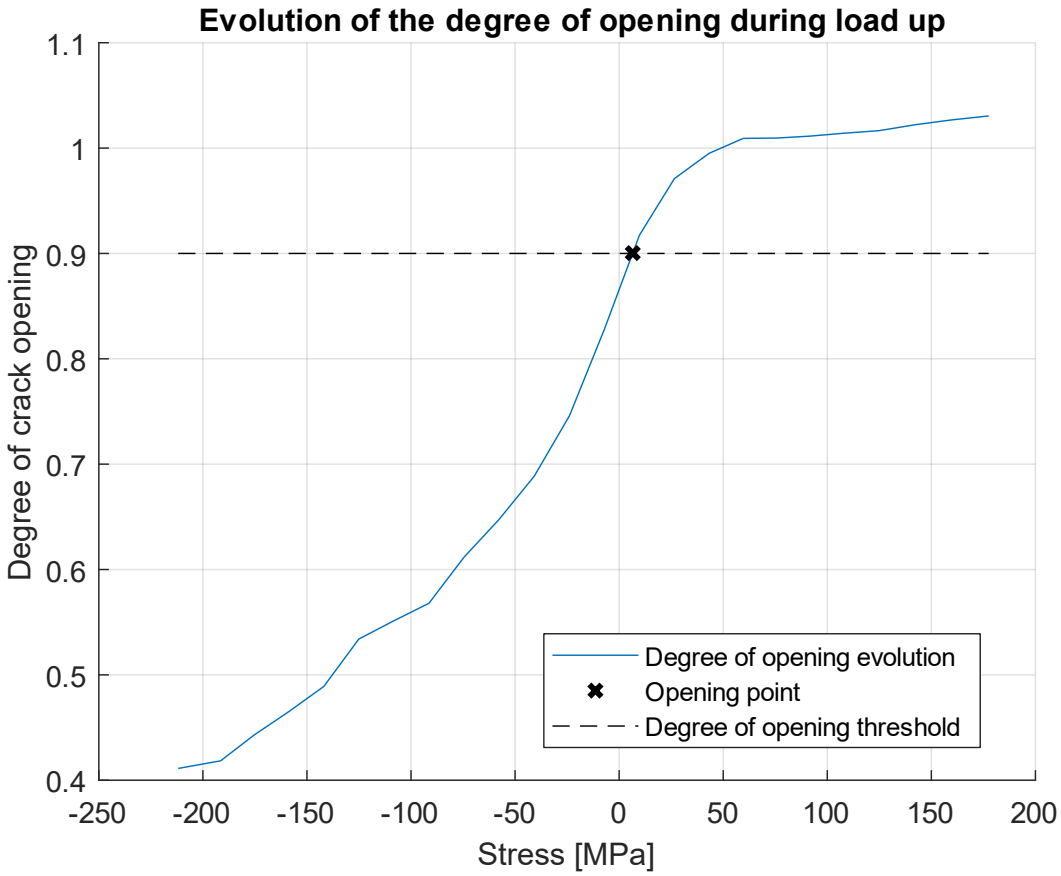

Figure 4: Illustration of the typical evolution of D during a ramp up of a cracked specimen.

Due to the measurement uncertainties and the inherent noise in the signals, it is often necessary to relax the set value of D when the crack is considered fully opened. As mentioned before, this point should be set to $D = 1$ for a fully opened crack, in the experimental evaluation this criterion is conveniently set to $D = 0.9$, meaning that the true effective stress intensity range is slightly overestimated for the experimental evaluation. The selection of an appropriate value of *D* for the crack opening criterion is a trade-off between reducing scatter in the determined crack opening force and minimizing the deviation from the force corresponding to a complete crack opening. An important aspect of this trade-off is the crack length limit above which crack opening evaluation is possible: Since the scatter of the determined crack opening force decreases with increasing crack length, it is possible to evaluate tests with large cracks using a crack opening criterion higher than 0.9. On the other hand, this would narrow the outcome of the testing.

4 Numerical crack opening evaluation

As mentioned before, crack opening estimations are challenging. A way to complement the experimental method is by means of a numerical simulation, which is performed under idealized conditions and the opening evaluation can be evaluated next to the crack tip and by means of several possible opening criteria. Specifically, while noise is limiting the value of D to ~0.9 for experimental evaluation, in a numerical context it is straightforward to calculate crack closure corresponding to D=1.

The FE-simulations were done in 2D under plane stress conditions. This assumption was deemed to fit the specimen geometries, shown in Figure 1, reasonably well. The choice of either plane strain or plane stress conditions could be argued and ideally, a 3D model should be used to better precision [12], although not without further additional issues [13]. All things considered, it was determined that the most cost-effective approach was a 2D model under plane stress conditions, given the relatively small thickness of the specimens, and the fact that the surface stress is more representative to crack growth rate.

It is well known that the size of the mesh is a key factor in the modelling of crack closure and the reader is referred to the work in [14] for more details. For this work, it was assumed that an element size of 50μm was sufficient to resolve crack closure with an acceptable resolution. This size of elements around the crack tip region is also in-line with the general recommendation for element size given in [15], which recommends 10 linear elements within the Dugdale's plastic zone. The used elements are 4-noded quadrilateral elements in the region where the crack grows. No remarkable differences in the results were found when 2nd order elements of the same size were tested and, all things considered, it was found that linear elements provided the most cost-effective results.

As the crack closure phenomenon is mostly driven by plasticity, it is not difficult to accept that the material model used throughout the simulations has a large impact on the outcome [16–18]. In this work, a perfect-plastic model was used. An important advantage of using such model in conjunction with plane stress assumption it that ratcheting is prevented. The flow stress values were obtained by numerically fitting the response of the finite element model to the global stress-strain data from the first two cycles of the experiments. The resulting flow stress values are 875 MPa at 20 ºC, 852 MPa at 100ºC, 690 MPa at 750ºC and 590 MPa at 850 ºC. Additionally, a creep material model was used in the simulations of the experiments under prolonged hold times. The creep model is based on a hyperbolic law, the parameters of which were obtained separately from this work based on smooth-specimens creep tests. Unfortunately, the actual parameters for the hyperbolic creep law are confidential intellectual property of Siemens and can not be disclosed in this paper.

The simulations to compute plasticity-induced crack closure are based on the node-release method, in which the crack is advanced by releasing one node at a time and at a given instance. For this work, the nodes are released at maximum load with two hold times in-between, c.f. Figure 5. The selection of the moment at which the node is released does somewhat change the outcome of the crack opening stress. Other authors claim that the node release should be at minimum load [19]. For this work, with the basis on that it is believed to better represent reality and to avoid numerical issues, the nodes are released at maximum load, a choice which is found also in [14,15,20].

The used method does not simulate the actual crack growth rate but rather it is used to predict the crack-tip opening stress and, with this information, it is possible to infer ΔK_{eff} as a function of crack length. The opening loads were monitored using two methods: compliance-based and crack-tip displacement. The former uses the same principles as described for the experimental evaluation of opening stress, using the displacements at the same location as the experimental strain gauge is located, as shown in Figure 6-a), allowing for a back-to-back comparison. The opening stress criterion for this method (see Equation 1) can be set to match the experimental evaluation or to any other arbitrary value; under the idealised conditions that a simulation provides, it is possible, in principle, to use an opening criteria of $D = 1$. The crack-tip displacement method is based on the displacement at the first node immediately behind the crack tip, as shown in Figure 6-b). The opening stress S_{op} is extracted at the instant where the node behind the crack tip shows a relative displacement greater than 0 with respect to the fixed plane. It is worth noting that in an ideal case, both methods are equivalent, if the degree of opening criteria is set to $D \approx 1$. Both methods require a relatively small time-step during the loading ramp to resolve the opening instant accurately, which for this work was set to fixed intervals of 1/100th of the ramp time. With this fine time-interval, it was found unnecessary to perform any interpolation to find the crack closure instant.

The numerical evaluation of ΔK_{eff} uses the opening ratios, $S_{op}/S_{\max}$ as a function of crack length obtained from the finite element simulation to calculate the expected ΔK_{eff} as;

$$\Delta K_{eff} = U \cdot \Delta K = \left(\frac{1 - \left({S_{op}}/{S_{max}} \right)}{(1-R)} \right) \Delta K \qquad 3$$

where S_{max} is the maximum nominal stress reached at the end of the cycle, R is the load ratio and ΔK is the full stress intensity factor range considering the maximum and minimum applied nominal stress in the specimen defined as;

$$\Delta K = K_{max} - K_{min} \qquad 4$$

The characterisation of the stress instensity factor, K, as a function of crack length was derived from a linear-elastic 3D crack propagation model for each specimen geometry.

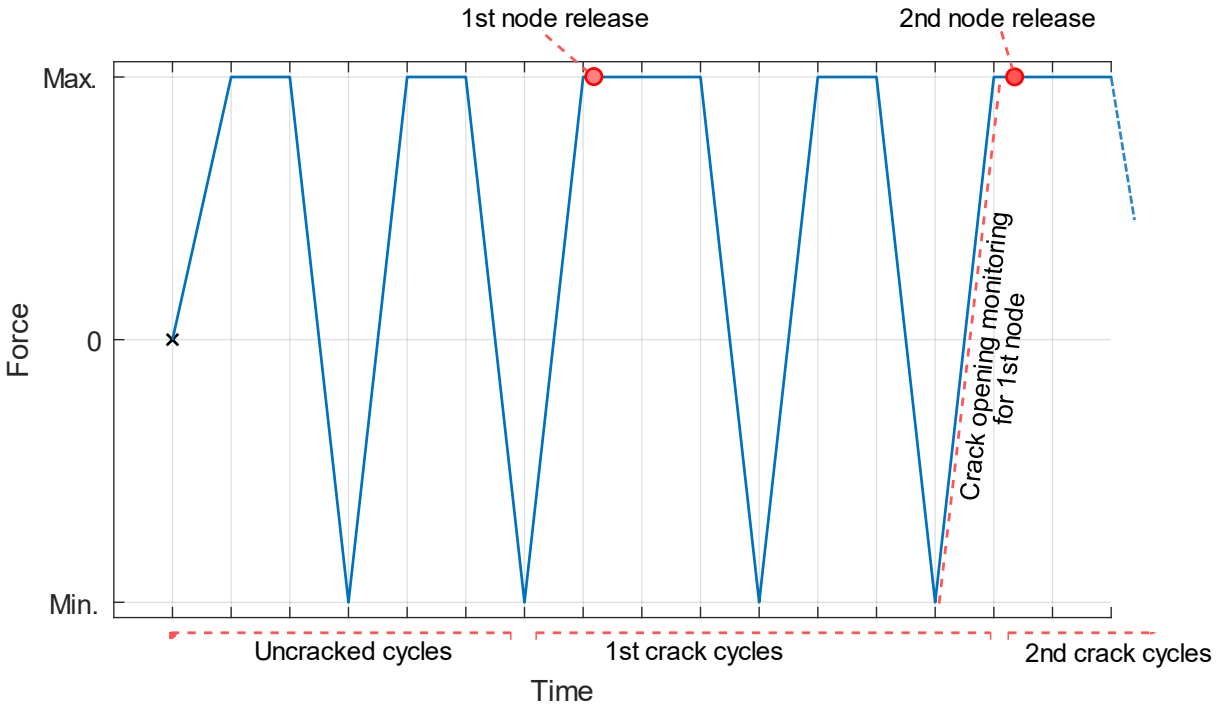

Figure 5: Schematic representation of the node release scheme.

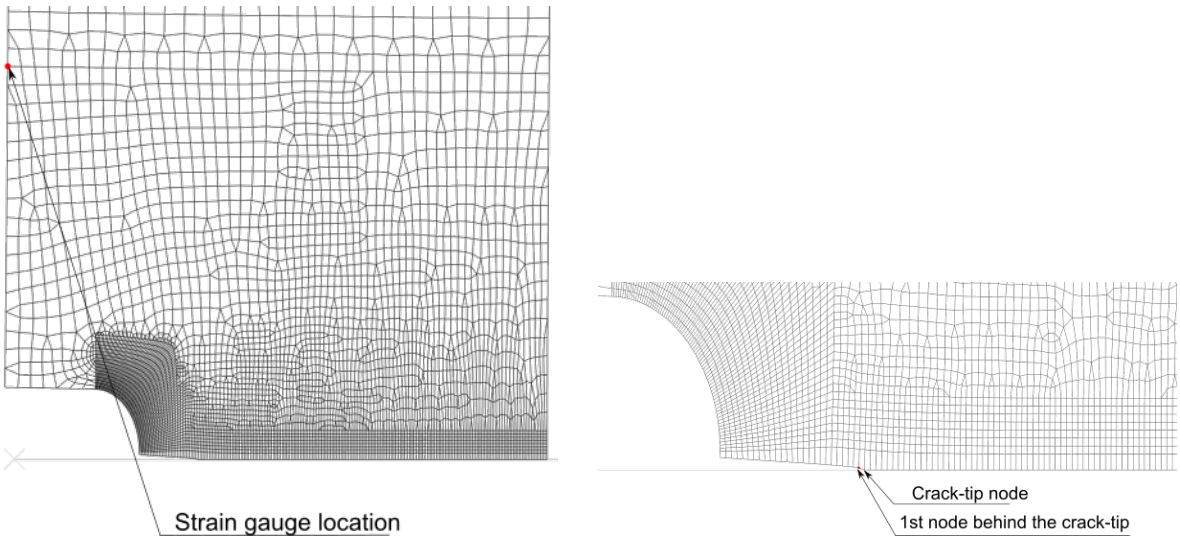

Figure 6: Crack-opening stress monitoring locations. a): Location used to monitor the strain-gauge displacement. b): Location to monitor the crack tip displacement.

5 Results

Experimental results

The guideline from ASTM [21] for tests with load ratios lower or equal to zero is to assume that the negative part of the stress-intensity factor interval does not influence the fatigue crack growth, as thus

$$\Delta K_{ASTM} = \max(K_{max}, 0) - \max(K_{min}, 0) \qquad 5$$

Under such an assumption, the experimental tests are plotted in Figure 7. It can be noted that the tests present distinguishable groups based on the length of the hold time: no hold, 1 hour and 6 hours, respectively.

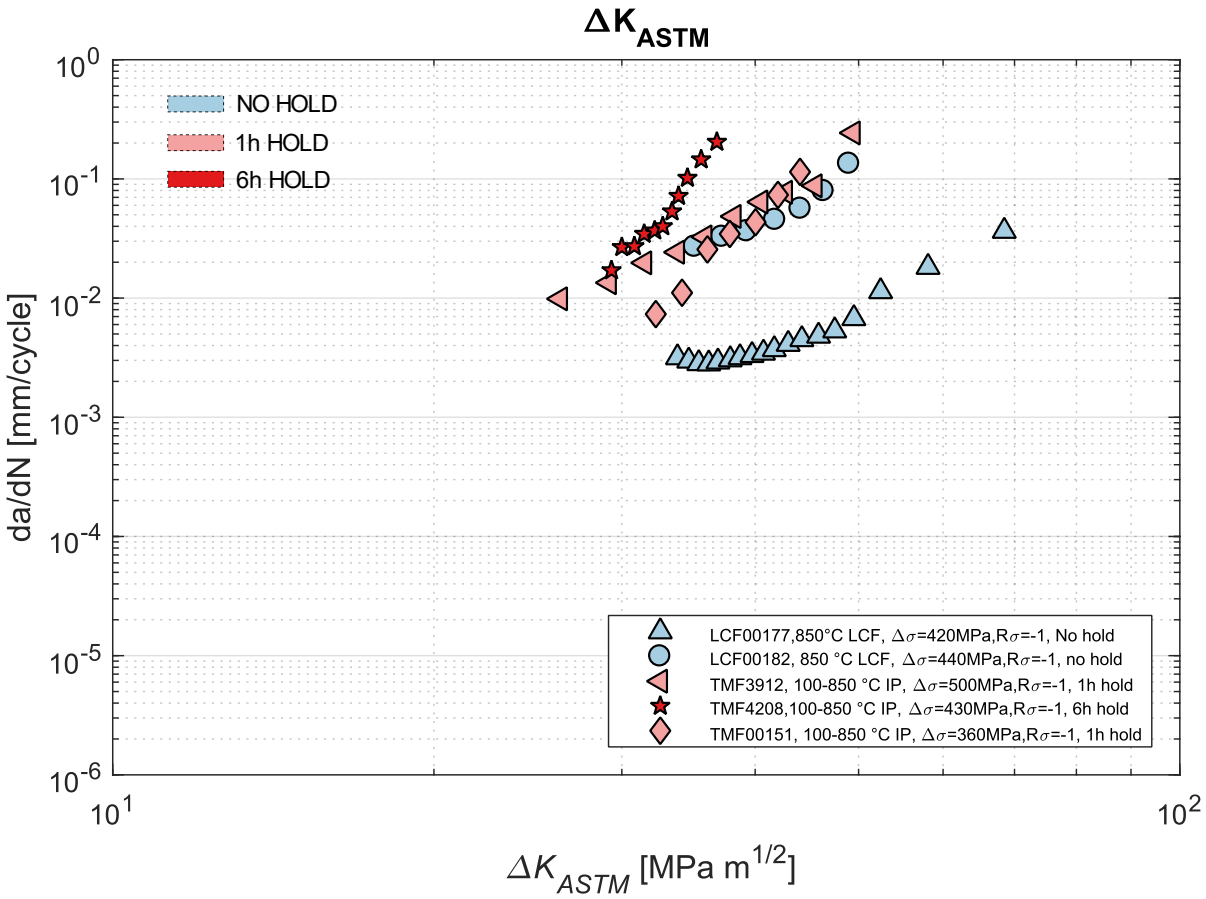

Figure 7: Experimental crack growth rates for the operational stress-intensity factor ΔK_{ASTM}.

The use of the aforementioned operational stress-intensity factor excludes any local crack-tip effects due to e.g. residual stress, crack-tip blunting or crack closure, which for cases with large compressive cycles might become non-conservative, as the crack may be open even under negative loading due to a combination of the presence of residual stress and crack closure effects. In these cases, an alternative approach, also included in the ASTM [21] code, is to use the full range of the stress-intensity factors, $\Delta K = K_{max} - K_{min}$. The experimental crack growth rate versus full range ΔK is shown in Figure 8.

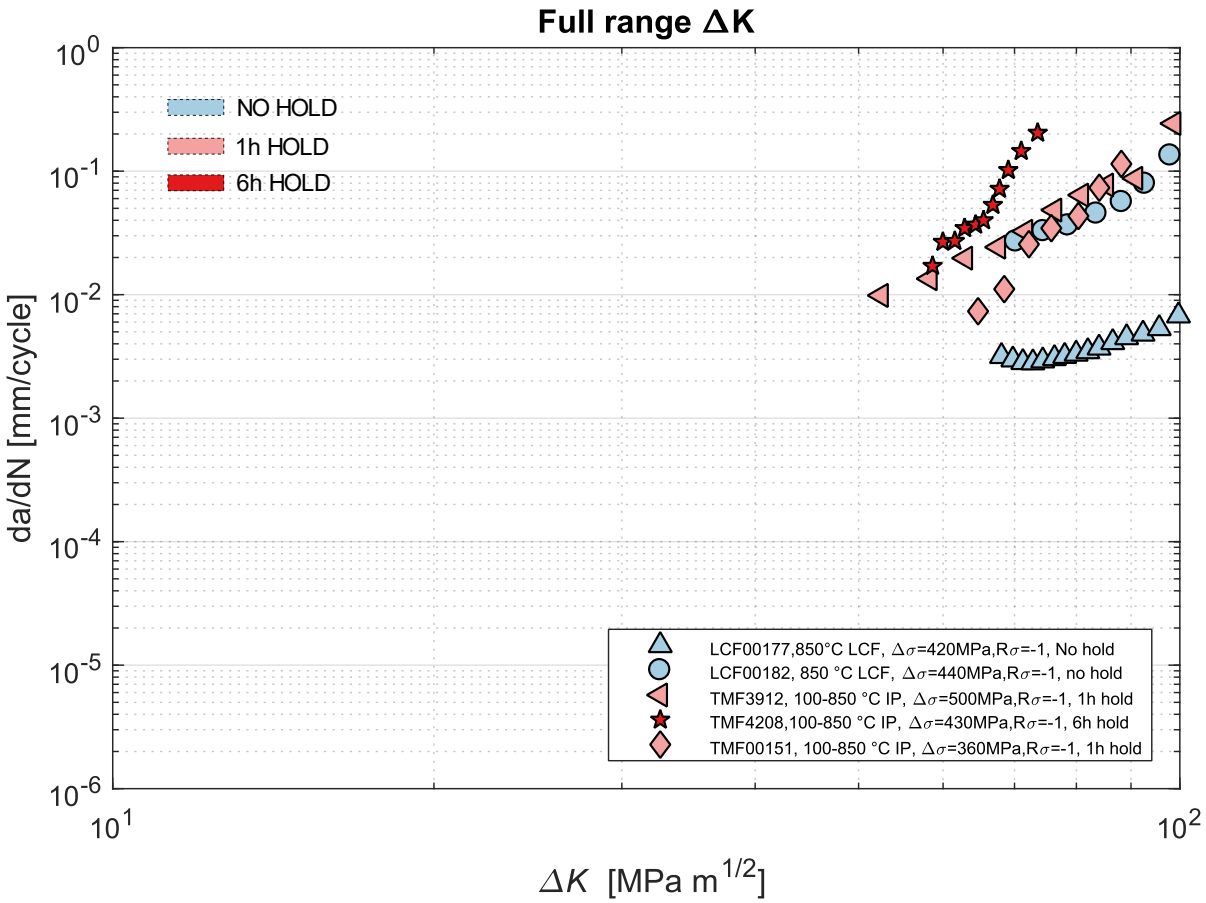

Figure 8: Experimental crack growth rates for the operational stress-intensity ΔK full range.

The results shown in Figure 8 using this operational stress-intensity range, also appear to be grouped according to the length of the hold times.

When the crack growth rates are plotted against the experimentally evaluated, effective stress-intensity range, see Figure 9, the results fall into a narrower band.

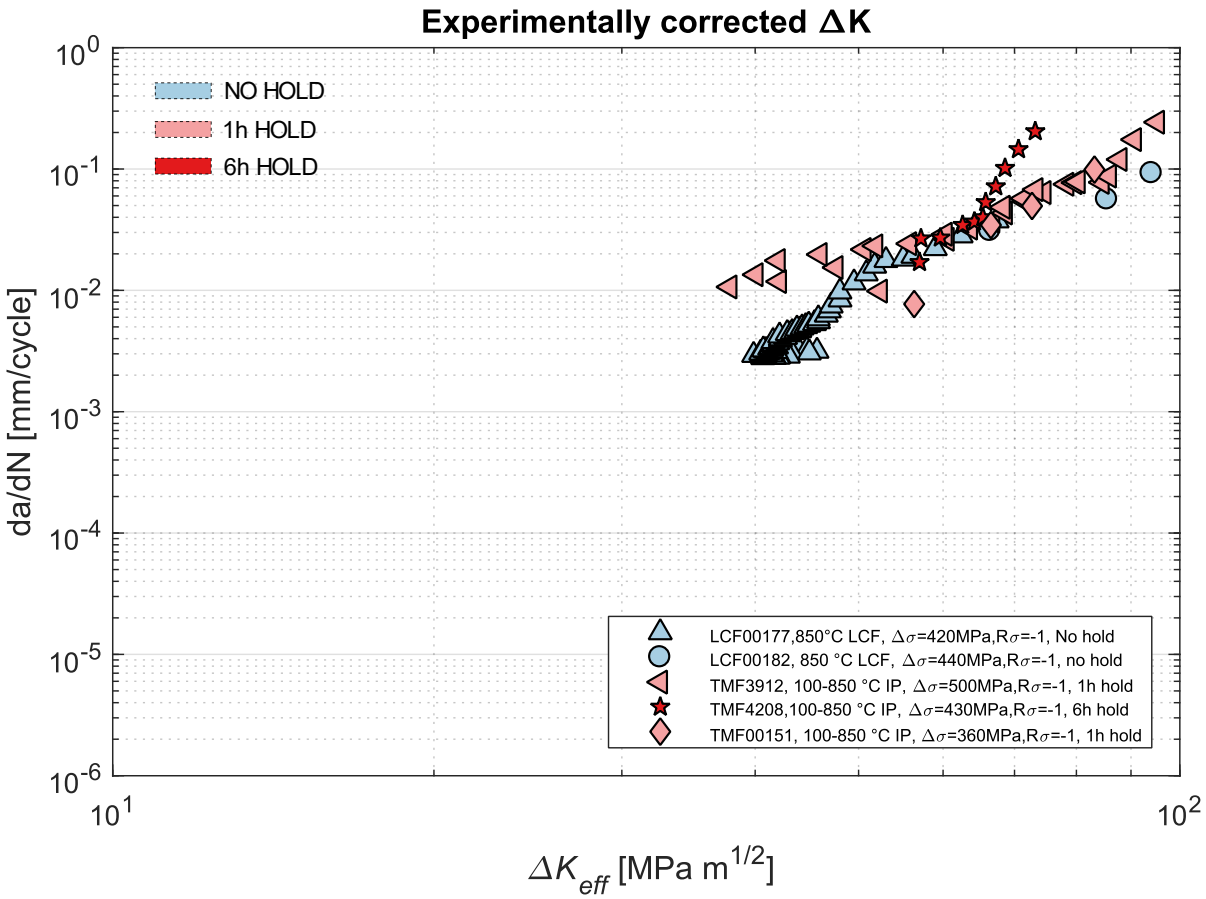

Figure 9: Experimental crack growth rates for the experimentally evaluated stress-intensity range, ΔK_{eff}.

The results in Figure 9 suggest that crack closure is a phenomenon present in these tests and, even though not the whole explanation, it can collapse the data to a narrower band. It is worth noting that, as mentioned in Section 3 in this work, the experimental evaluation of crack closure requires a relaxation of the opening criterion ($D = 0.9$) which generally leads to an overestimation of ΔK_{eff}.

Validation of the numerical results

The validation of the numerical results is done in two steps; first, the simulations are validated with respect to the experiments using the same compliance-based methodology and associated parameters that was used to estimate crack closure experimentally. Afterwards, with the knowledge of having comparable results between the simulations and the experiments, it is possible to raise the criterion for the degree of opening from $D = 0.9$ to $D = 1$ for the simulations, and verify that the results using the crack-tip criterion are comparable to the results found by using the compliance-based method for *D*=1.

The experimentally obtained effective stress intensity range is in Figure 10 compared to the numerically obtained one for all test, which shows that, with marginal differences, the simulated results are comparable to the experimentally obtained ones. Based on these results it can be stated that the simulation captures the experimental results well, for the same degree of opening criterion, $D = 0.9$.

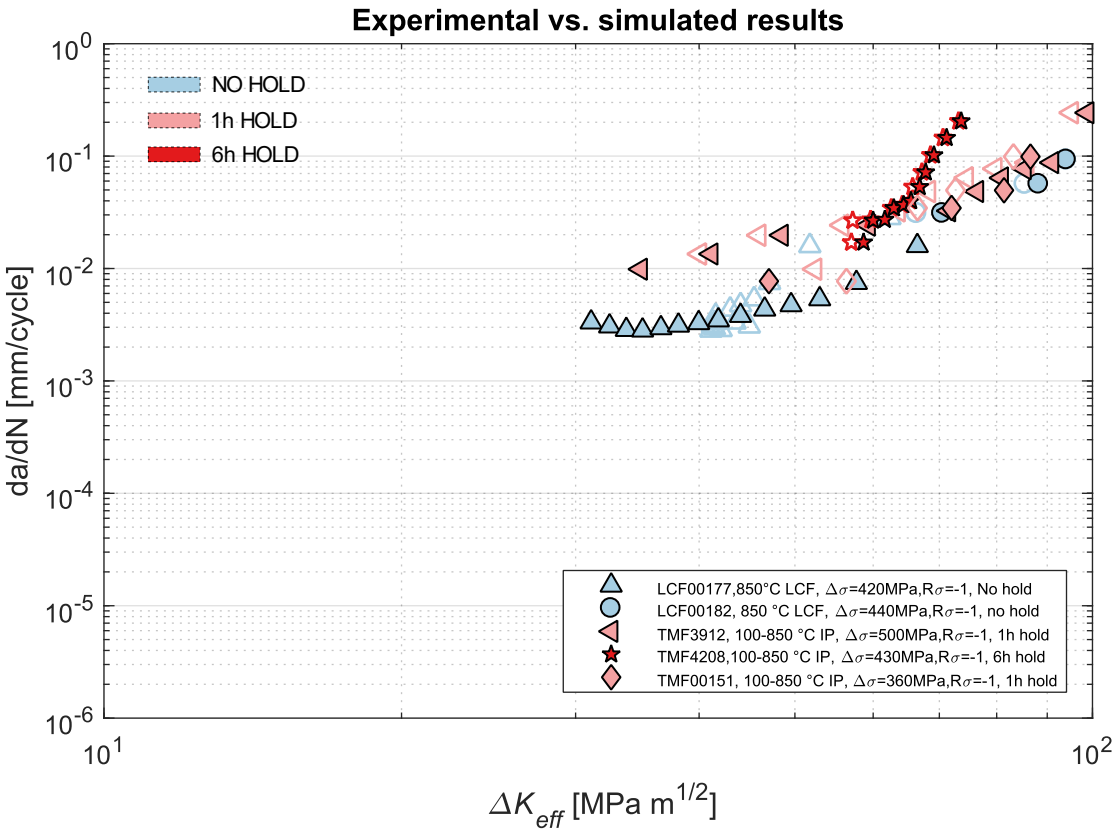

Figure 10: Comparison of the experimental and simulated effective ΔK. The filled markers correspond to the numerically obtained values. Empty markers correspond to the experimental counterpart.

A comparison of the experimentally and numerically found values of the ratio U (c.f. Equation 3) with respect to the crack length is shown in Figure 11. From this plot it is possible to infer that most of the experimental values are well represented by the numerical simulation, although in some cases, not for the full range. An observation that can be made based on this figure is that under load ratios of -1, the operational stress-intensity factor ΔK_{ASTM}, corresponding to a value of $U = 0.5$, is better suited to the no hold cases than it is for the tests with extended hold times.

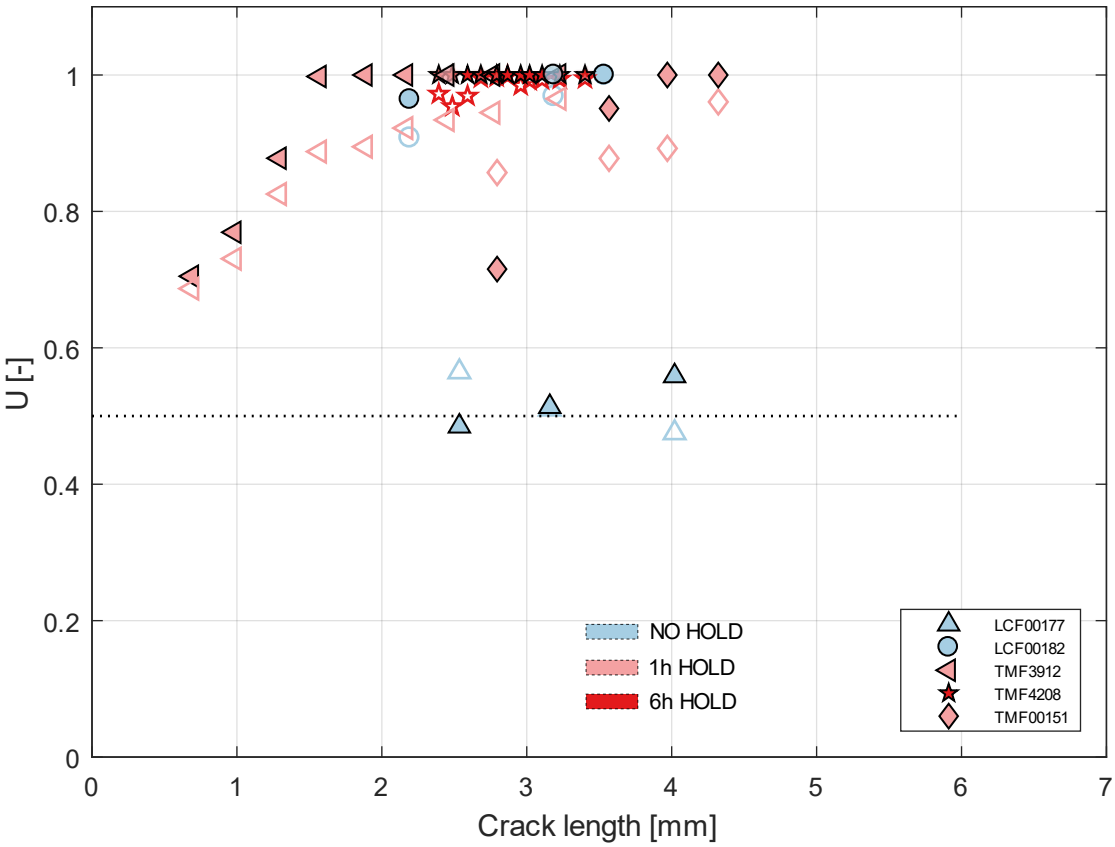

Figure 11: Comparison of the experimental and simulated values of U as a function of crack length. The filled markers correspond to the numerically obtained values. Empty markers correspond to the experimental counterpart.

With the knowledge of having a simulation technique that can capture the experimental results well, it is possible to stretch the criterion for the compliance-based method. Ideally, a fully open crack is reached at the instant when *D* reach the value of 1. Conversely, a fully open crack is reached at the instant where the flank immediately behind the crack tip is no longer in contact with its reciprocal crack-face, meaning that both methods should converge for values of *D* close to 1.

For illustration purposes, the results in Figure 12 show the difference of these two criteria for values of D 0.9 and 1 from the simulation of a 1h hold test experiment, showing that both methods converge for $D = 1$ and what that means is that it is possible to use the crack opening criterion for the crack tip as a more precise methodology to estimate the actual crack closure for each test.

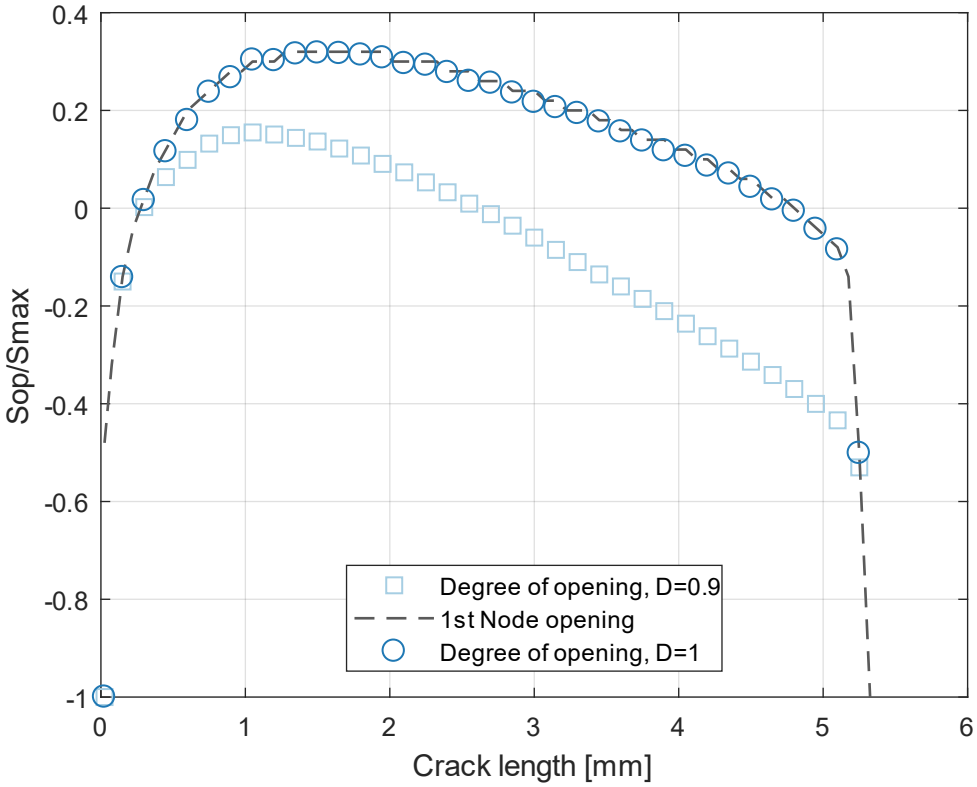

Figure 12: Validation of the numerical crack opening criteria for the crack-tip.

Numerical results

The values of the crack opening stress ratio $S_{op}/S_{\max}$ for each test are obtained from the numerical simulations and are summarized in the plots in Figure 13. With the characterisation from the simulations of the opening stress ratio as a function of the crack length, it is possible to use Equation 3 to evaluate the experiments with the opening stress ratio obtained from the simulations.

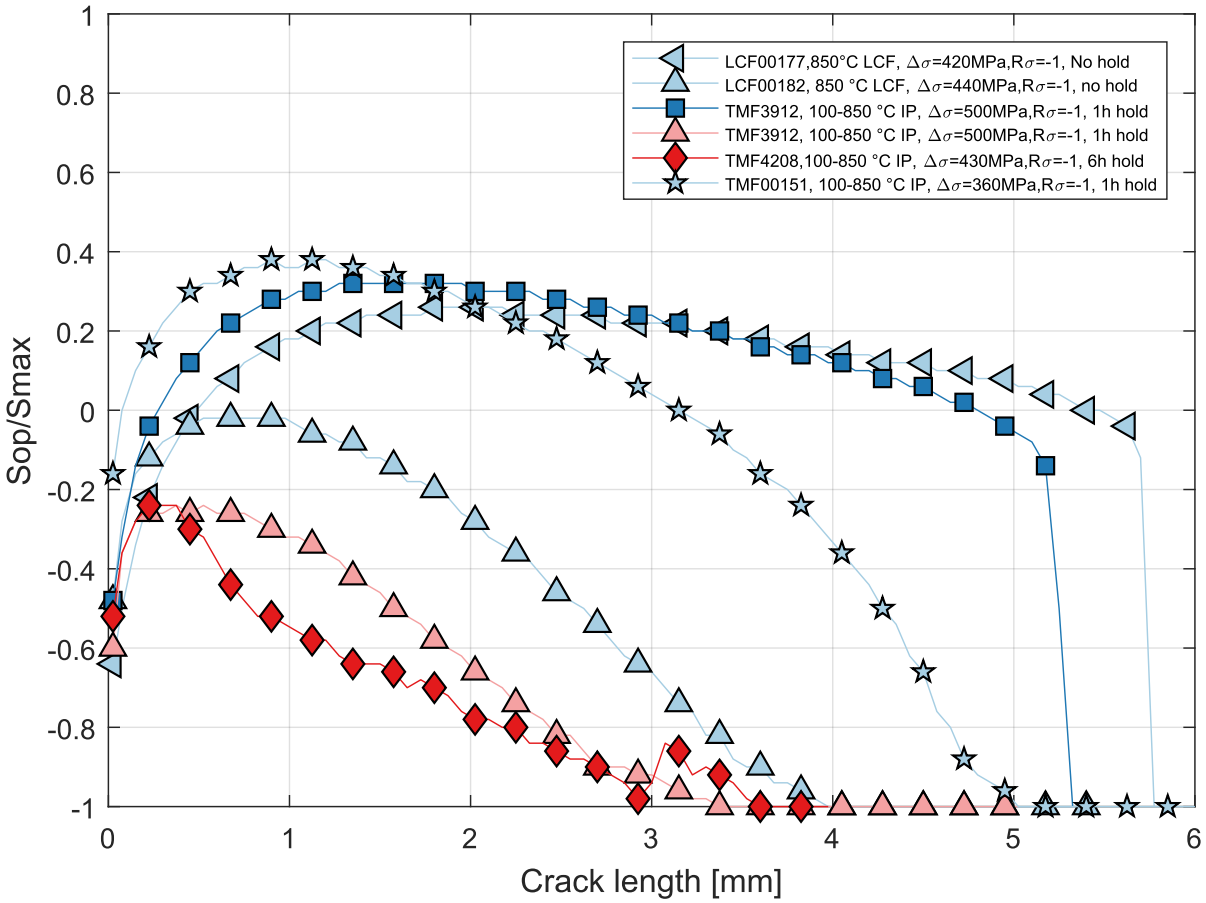

Figure 13: Numerically inferred crack opening ratios using the opening criterion for the crack-tip.

The numerical results are first evaluated following an identical methodology as for the experimental procedure, that is, using a compliance-based method to estimate the moment at which the crack starts to be open based on the displacements in the strain gauge (see Figure 6-a). These results are used as means to verify that the experimental and numerical methods result are comparable. The results for the numerically estimated effective stress-intensity range ΔK_{eff} are shown in Figure 14.

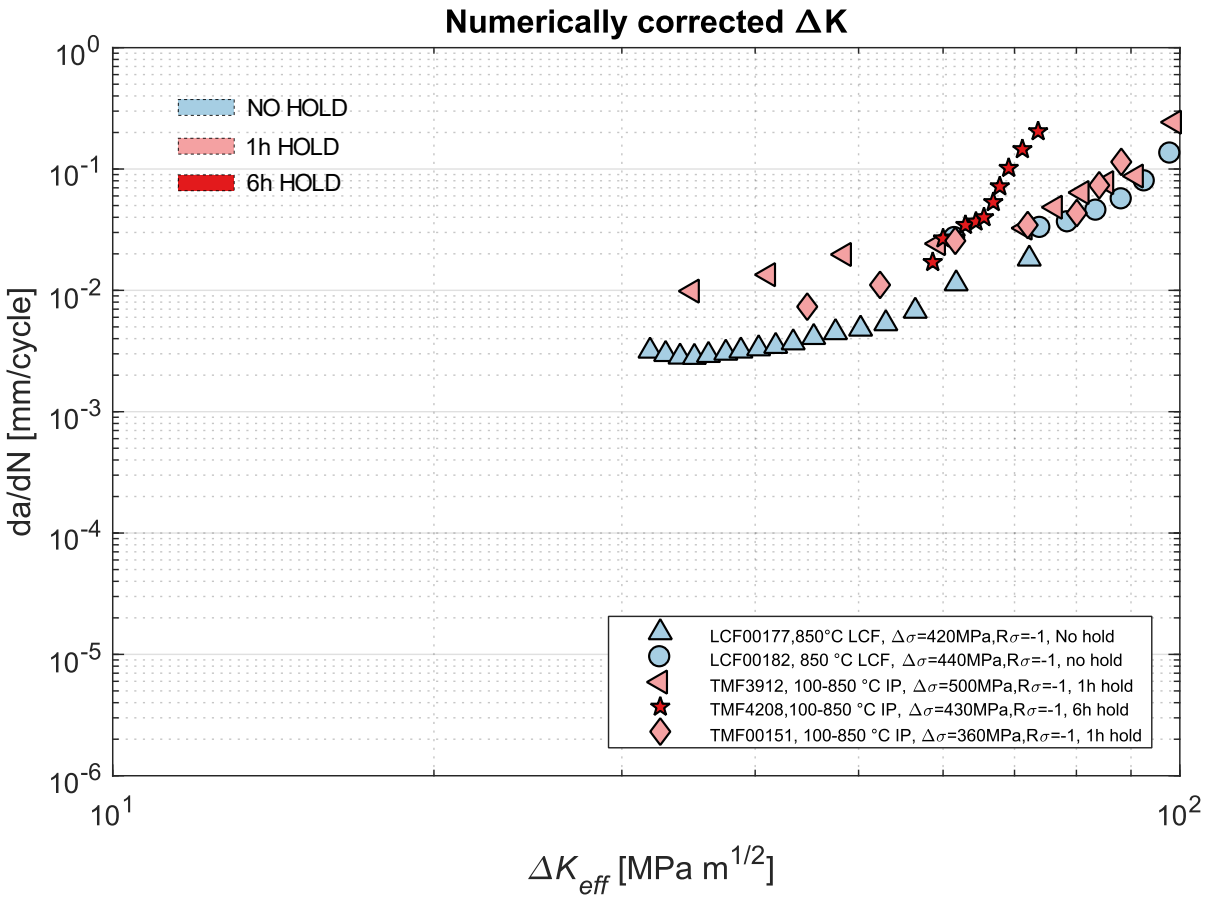

Figure 14: Crack growth rates versus the numerically estimated compliance-based (D=0.9) effective stress-intensity range, ΔK_{eff}.

The results from Figure 14 can be compared to the experimental results included in Figure 9, showing that the experimental and numerical results are fairly similar, concluding that the numerical method can be used to describe the experimental results with some degree of confidence. This is, in fact, the same verification already presented in Figure 10.

As discussed in the previous section of this work *Validation of the numerical results*, the simulations agree well with the experiments, and it has been shown that it is possible to rely on the simulations to extract the crack opening stress more precisely when using the crack-tip displacement criterion. The results based on the numerically obtained opening stress using the latter criterion are shown in Figure 15.

The results show that the experimental and numerical evaluation in Figure 9 and Figure 14 are fairly similar, for the cases in which both evaluations share the same method to infer the opening stresses. On the other hand, when comparing the experimental evaluation in Figure 9 and the numerically obtained estimation of the crack opening stress using the crack-tip method in Figure 15, the results for some tests show an obvious trend to diverge from the experimentally obtained values. This is due to the systematic overestimation of ΔK_{eff} on the experimental procedure discussed before.

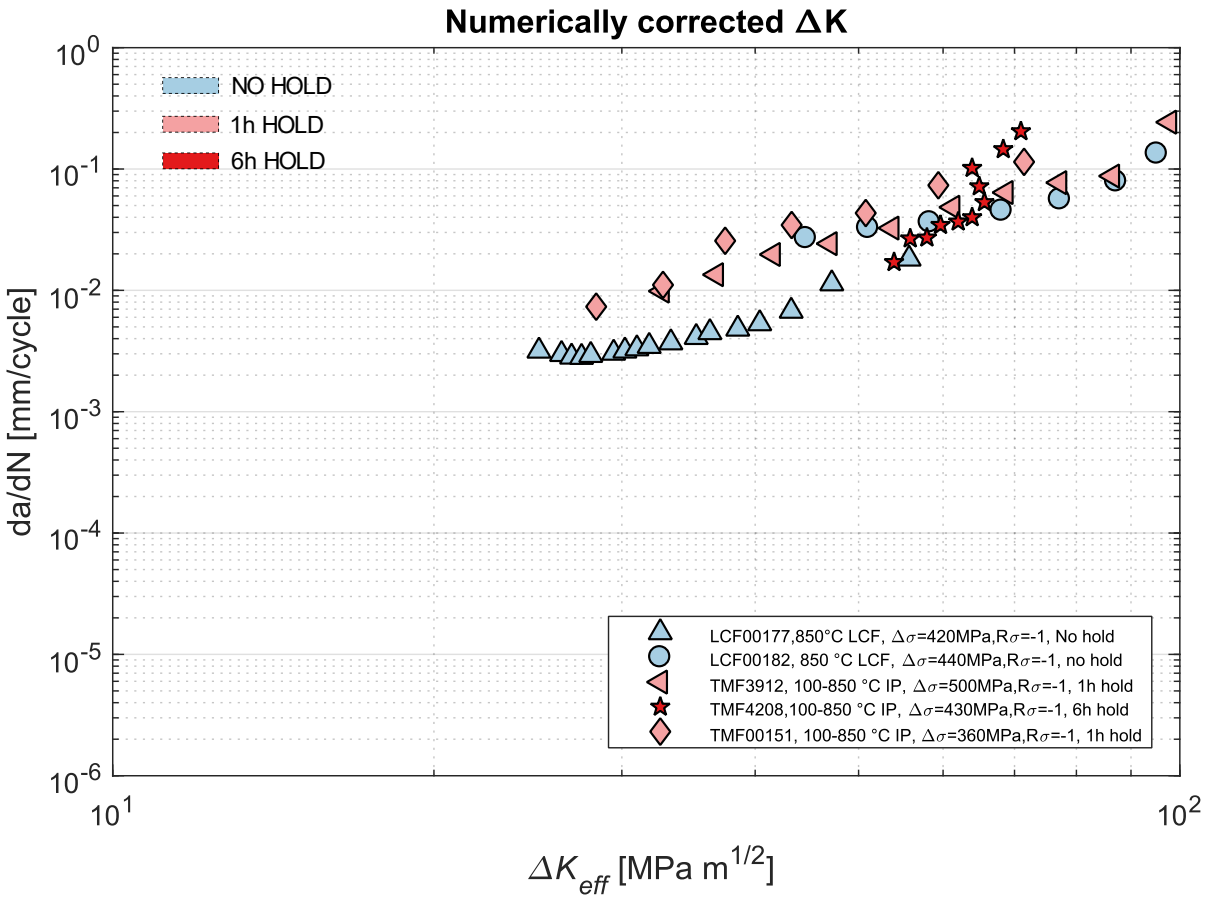

Figure 15: Crack growth rates versus the numerically estimated crack-tip based effective stress-intensity range, ΔK_{eff} with respect to the crack tip.

For the sake of comparison, the numerically corrected ΔK_{eff} is used to obtain a regression line following a Paris model. This regression line is used to show in Figure 16 the excellent qualitative similarity between the experimentally and numerically obtained ΔK_{eff}. Note that by means of using the numerical correction, the model captures most of the tests within a factor of 3.

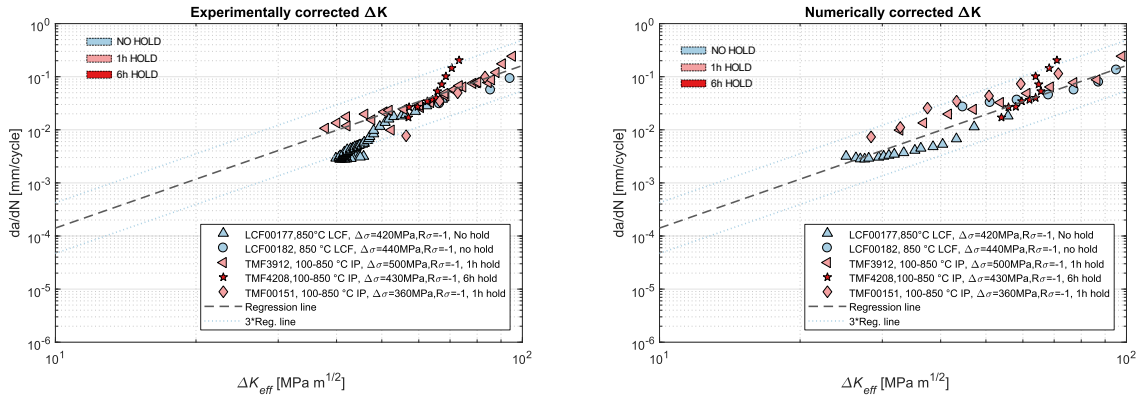

Figure 16: Qualitative comparison between the experimental and numerically obtained ΔK_{eff} as an operational stress-intensity factor.

6 Discussion

The results suggest that for this material and loading conditions, crack closure effects can, to a large degree, explain the crack growth rate under TMF conditions with different hold times. Comparing the effects of crack closure on this material (Inconel 792) with the ones described in [4] (nickel-based, single crystal superalloy), it is evident that crack closure has a lesser effect on this material and tests. The reasons behind this may be a combination of many factors, such as the different set of material properties, the effects of crystallographic texture, time-dependent behaviour, or damage evolution at the crack tip among others. It is evident that, albeit not being the only phenomenon in play, the effects of crack closure are of primary importance for this material, which on its own, is a main conclusion from this work.

The length of the hold times has a large impact on the importance of the crack closure, although it needs to be complemented with the magnitude of the stress range; a no-hold test might present stronger crack closure effects than a 6h test given the load is large enough. The impact of crack closure is highly transient and complex and is often counterintuitive and difficult to predict without the aid of a simulation.

It has been shown that the relatively simple simulations presented in this work can capture the behaviour of crack closure estimated on the experiments well. Additionally, the numerical simulations can be used to characterise crack closure with respect to the local crack tip behavior, which leads to more precise results than a compliance-based method.

It is worth discussing that most of the experiments are carried out in blocks, having a combination of LCF and TMF testing in different orders and with different load magnitudes. These changes in the loading regime will, in fact, have an impact on the crack closure levels as is schematically shown in Figure 17. In this figure, the blue line is a simulation carried out with the final relevant loading conditions of the test, excluding the pre-cracking cycles. If the pre-cracking cycles are also included in the simulation (dashed red line), a transition zone appears until it converges with the crack closure levels obtained excluding pre-cracking cycles. For practical reasons, and due to the fact that the transition zones are often relatively small, the simulations were performed excluding previous cycles, although at some instances, accounting for the whole loading history of the test might lead to slightly better results.

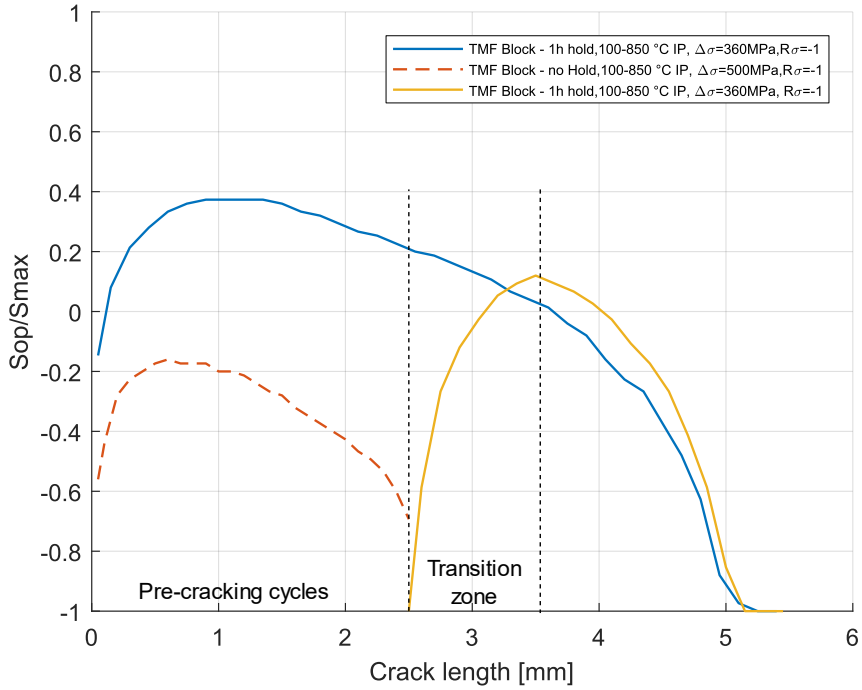

Figure 17: Schematic representation of the crack closure transition between loading blocks.

The tests rely heavily on stiffness drop measured at the extensometer. This metric is used to estimate the average crack length and the crack opening stress. The crack length measurement has been thoroughly investigated by other authors and has been proven to work well with a good accuracy for this

type of tests, considering the measurements on the heat tints and the side pictures. There are still some questions about the performance of this method to measure crack lengths for cases where the crack branches or kinks heavily, as is the case for some of the tests in this work, as for example the one shown in Figure 18. It is also unknown how a possible creep-damaged zone may impact the estimation of the crack length.

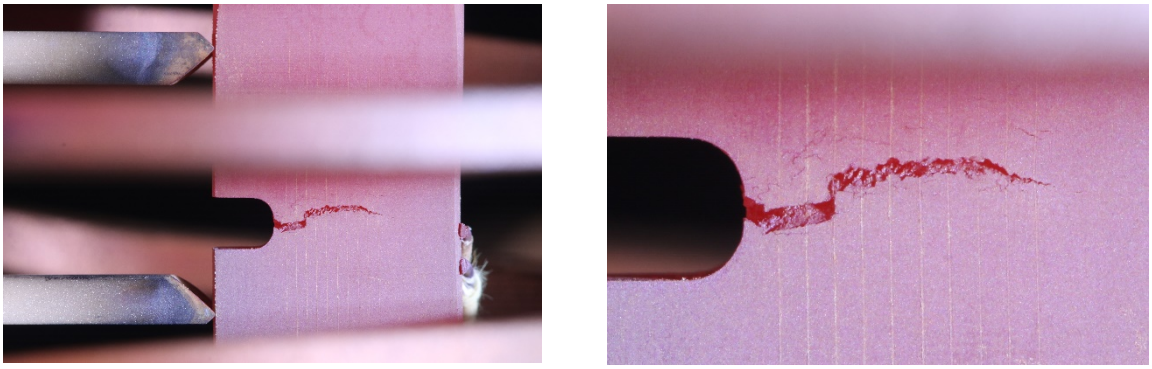

Figure 18: Detail of the crack branching and kinking during the test TMF00151. Side-picture taken at the late stages of the test.

Finally, it appears that roughness-induced crack closure is of less importance for these experiments. This suggestion is inferred from the fact that the simulations and the experimental crack opening stress agrees well despite not accounting for roughness in the simulations.

7 Conclusions

The main conclusions that can be drawn from this work are as follows:

- The experiments show that the crack closure phenomenon has a primary impact on crack growth behaviour for this material and test conditions.
- Creep and oxidation damage might complement crack closure to fully explain the crack growth rate under different loading and temperature regimes, although for these tests the results suggest that it is not of primary importance.
- The simulated plasticity/creep crack closure levels and the related ΔK_{eff} agree well with the experimentally obtained ones for the same crack opening criterion. This also suggests that roughness-induced crack closure has an insignificant role in these experiments.
- The numerical model can be used to improve the experimental data by obtaining the crack opening levels with respect to the crack tip.
- The numerically obtained values of ΔK_{eff} encapsulate the experiments within 3 times the mean value of the crack growth rate.

Acknowledgements

This research has been funded by the Swedish Energy Agency and Siemens Industrial Turbomachinery AB through “Turbines for Future Energy Systems” (Turbiner för framtidens energisystem), Grant No. 44100-1, the support of which is gratefully acknowledged.

References

[1] Elber W, Fatigue crack closure under cyclic tension, Eng. Fract. Mech. (1970). doi:10.1016/0013-7944(70)90028-7.

[2] Elber W, The significance of fatigue crack closure, ASTM Spec. Tech. Publ. (1971).

[3] V. Norman, S. Stekovic, J. Jones, M. Whittaker, B. Grant, On the mechanistic difference between in-phase and out-of-phase thermo-mechanical fatigue crack growth, Int. J. Fatigue. 135 (2020) 105528. doi:10.1016/j.ijfatigue.2020.105528.

[4] F. Palmert, J. Moverare, D. Gustafsson, Thermomechanical fatigue crack growth in a single crystal nickel base superalloy, Int. J. Fatigue. 122 (2019) 184–198. doi:10.1016/j.ijfatigue.2019.01.014.

[5] P. Almroth, D. Gustafsson, J. Loureiro-Homs, K. Simonsson, Out-of-phase thermo-mechanical fatigue crack growth and the effect of the compressive minimum load level on crack closure at notches, Accepted for publication in Int. J. of Fatigue.

[6] J. Loureiro, D. Gustafsson, P. Almroth, K. Simonsson, R. Eriksson, D. Leidermark, Accounting for Initial Plastic Deformation for Fatigue Crack Growth in Turbine Blading Components, in: Proc.\ 13th Int. Conf. Mech. Behav. Mater. ICM-13, RMIT University Melbourne, Australia, 2019.

[7] J. Loureiro-Homs, D. Gustafsson, P. Almroth, K. Simonsson, R. Eriksson, D. Leidermark, Accounting for initial plastic deformation for fatigue crack growth predictions under TMF loading condition, Int. J. Fatigue. (2020). doi:10.1016/j.ijfatigue.2020.105569.

[8] E. Salvati, H. Zhang, K.S. Fong, X. Song, A.M. Korsunsky, Separating plasticity-induced closure and residual stress contributions to fatigue crack retardation following an overload, J. Mech. Phys. Solids. 98 (2017) 222–235. doi:10.1016/j.jmps.2016.10.001.

[9] R. Pippan, W. Grosinger, Fatigue crack closure: From LCF to small scale yielding, Int. J. Fatigue. 46 (2013) 41–48. doi:10.1016/j.ijfatigue.2012.02.016.

[10] D. Ewest, P. Almroth, B. Sjödin, K. Simonsson, D. Leidermark, J. Moverare, A modified compliance method for fatigue crack propagation applied on a single edge notch specimen, Int. J. Fatigue. 92 (2016) 61–70. doi:10.1016/j.ijfatigue.2016.06.023.

[11] J. Moverare, Thermomechanical fatigue crack growth in a cast polycrystalline superalloy,

MATEC Web Conf. 14. 19004 (2014).

[12] A. Gonzalez-Herrera, J. Zapatero, Tri-dimensional numerical modelling of plasticity induced fatigue crack closure, Eng. Fract. Mech. 75 (2008) 4513–4528. doi:10.1016/j.engfracmech.2008.04.024.

[13] H. Alizadeh, D.A. Hills, P.F.P. de Matos, D. Nowell, M.J. Pavier, R.J. Paynter, D.J. Smith, S. Simandjuntak, A comparison of two and three-dimensional analyses of fatigue crack closure, Int. J. Fatigue. 29 (2007) 222–231. doi:10.1016/j.ijfatigue.2006.03.014.

[14] A. González-Herrera, J. Zapatero, Influence of minimum element size to determine crack closure stress by the finite element method, Eng. Fract. Mech. 72 (2005) 337–355. doi:10.1016/j.engfracmech.2004.04.002.

[15] R.C. McClung, H. Sehitoglu, On the finite element analysis of fatigue crack closure-1. Basic modeling issues, Eng. Fract. Mech. 33 (1989) 237–252. doi:10.1016/0013-7944(89)90027-1.

[16] S. Pommier, Influence of a negative R ratio on the creep-fatigue behaviour of the N18 nickel base superalloy, Fatigue Fract. Eng. Mater. Struct. 20 (1997) 93–107. doi:10.1111/j.1460-2695.1997.tb00405.x.

[17] S. Pommier, Plane strain crack closure cyclic hardening, Eng. Fract. Mech. 69 (2001) 25–44. doi:10.1016/S0013-7944(01)00061-3.

[18] S. Pommier, P. Bompard, Bauschinger effect of alloys and plasticity-induced crack closure: A finite element analysis, Fatigue Fract. Eng. Mater. Struct. 23 (2000) 129–139. doi:10.1046/j.1460-2695.2000.00259.x.

[19] G.P. Potirniche, Characterization of creep- fatigue crack growth in alloy 709 and prediction of service lives in nuclear reactor, U.S. Dep. Energy. (n.d.).

[20] R.C. McClung, H. Sehitoglu, On the finite element analysis of fatigue crack closure-2. Numerical results, Eng. Fract. Mech. 33 (1989) 253–272. doi:10.1016/0013-7944(89)90028-3.

[21] ASTM E647-13, Standard Test Method for Measurement of Fatigue Crack Growth Rates, Am. Soc. Test. Mater. (2013)